Time-resolved differential transmission in MOVPE-grown ferromagnetic InMnAs

M. Bhowmick, T. R. Merritt, and G. A. Khodaparast*
Department of Physics, Virginia Tech, Blacksburg, Virginia 24061, USA

Bruce W. Wessels
Materials Research Center, Northwestern University, Evanston, Illinois 60208, USA

Stephen A. McGill
National High Magnetic Field Laboratory, Florida State University, Tallahassee, FL 32310, USA

D. Saha, X. Pan, G. D. Sanders, and C. J. Stanton
Department of Physics, University of Florida, Gainesville, Florida 32611, USA
(Received 6 December 2011; revised manuscript received 3 February 2012; published 27 March 2012)

We measured time-resolved differential transmission in InMnAs for different pump/probe schemes as a function of temperature, laser fluence, and external magnetic field. We observed tunability of the carrier relaxation time. In addition, we found that the sign of the differential transmission changed as a function of probe wavelength. The electronic structure for InMnAs was calculated for $\mathbf{B} = 0$, using an eight-band $\mathbf{k}\cdot\mathbf{p}$ model, which includes conduction and valence band mixing as well as coupling of electrons and holes to the magnetic Mn impurities. This allows us to explain some of the carrier dynamics and the sign changes in the differential transmission.

DOI: 10.1103/PhysRevB.85.125313 PACS number(s): 75.50.Pp, 73.40.Kp

I. INTRODUCTIONs

Narrow gap ferromagnetic semiconductors (NGFS) such as InMnAs have significant potential for applications in infrared spin photonics and spin transport devices due to their small energy gap and much higher electron and hole mobilities relative to other III-Mn-V ferromagnetic semiconductors. The first III-V NGFS, InMnAs, was prepared by MBE with a Curie temperature T_c on the order of 10 K. Subsequent fabrications demonstrated a T_c closer to 90 K.[1] A low-temperature, MBE technique was nearly exclusively used to prepare InMnAs thin films; although, MOVPE, an alternative technique demonstrated that a single phase magnetic InMnAs compound could be deposited at 500 °C, much higher than that used in MBE.[2,3]

Furthermore, the MOVPE technique demonstrated that the films are ferromagnetic with a T_c of 330 K.[3,4] The Rudermann-Kittel-Kasuya-Yosida (RKKY) mechanism, where free holes mediate the ferromagnetism, is indeed favored in NGFS, while a small hole effective mass m_h results in a long interaction distance and effective exchange coupling. The hole effective Bohr radius in NGFS suggests a large enough overlap with the Mn-induced hole wave functions to stabilize ferromagnetism even for small Mn contents.[5] The ferromagnetic states were measured using several techniques reported earlier.[2–4,6]

In this work, several time-resolved differential transmission (TRDT)[7–9] schemes were employed to provide insight into the time scales and the nature of the interactions in MOVPE grown ferromagnetic InMnAs. We demonstrate the sensitivity and tunability of the carrier dynamics to the initial excitation region as well as the final states that are probed. The MOVPE-grown InMnAs structure is an 800-nm thick film with a Mn content of ∼4%, a hole concentration $p = 1.35 \times 10^{18}$ cm^{-3}, and a mobility of 142 cm^2/V s with the T_c above room temperature. The details of the growth conditions are described in Refs. 3 and 4. Probing the dynamical behavior of nonequilibrium carriers created by intense laser pulses can provide valuable information about different scattering mechanisms and the band structure. Time-resolved spectroscopy can help us to understand the relaxation of photoexcited carriers; where after the initial excitation, the nonequilibrium population of electrons and holes can relax by a series of scattering processes including carrier-carrier and carrier-phonon scattering.

Most of the understanding of carrier relaxation in MBE-grown narrow gap (III,Mn)V ferromagnetic structures has been based on two-color differential reflectivity spectroscopy with pump and probe pulses ranging from 1.2–2 μm and 650–850 nm, respectively.[10–13] In the reported measurements, rapid change of the differential reflectivity was observed and ascribed to a fast disappearance of photoinduced free carriers through ultrafast trapping by midgap states. The carrier relaxation time reported in the MBE grown InMnAs[12] demonstrated a similar time scale as an InAs film under similar experimental conditions.[14] Fast relaxation in the differential reflectivity patterns of relaxation dynamics are commonly seen in low-temperature-grown III-V semiconductors. The extracted information from the differential reflectivity measurements can be affected by multireflections in multilayer structures.

It is important to emphasize that our studies are unique in being able to investigate carrier dynamics in ferromagnetic semiconductors. That is because our InMnAs samples are on a GaAs substrate. Photoexcitation by the 800 nm pump pulse creates the majority of carriers in the InMnAs part of the sample with only a few carriers being excited near the band edge in the GaAs layer. In contrast, InMnAs[12] was previously grown on a GaSb buffer layer. Photoexcitation by the pump created substantial carriers in this buffer layer making it difficult to separate out the relaxation dynamics of the magnetic InMnAs layer from the GaSb buffer layer. In addition, GaMnAs samples are grown on a GaAs substrate.

Photoexcitation by the pump pulse creates carriers both in the GaMnAs layer as well as the GaAs substrate and again, one can not separate out the relaxation dynamics of the carriers in the magnetic layer from that in the nonmagnetic layer. We demonstrated the tunability of carrier dynamics and relaxation time with characteristics not reported in the MBE grown InMnAs[12] and InAs.[14] Examples of our measurements are presented here.

II. DEGENERATE DIFFERENTIAL TRANSMISSION

In our degenerate TRDT pump/probe measurements, the laser source was a difference frequency generator (DFG), which mixes the signal and idler beams from an optical parametric amplifier (OPA). The OPA itself was pumped by an amplified Ti:sapphire oscillator with a repetition rate of 1 KHz. The pulses had a duration of ∼100 fs defining the resolution of the measurements with the ratio of the pump:probe of 1000:1. Both beams were focused onto the sample with a spot size of around 150–200 μm for the probe and slightly larger for the pump. The differential transmissivity as a function of the time delay between the pump and probe pulses was measured using a liquid nitrogen-cooled Mercury Cadmium Telluride (MCT) detector.

Figure 1(a) shows examples of our degenerate TRDT in the InMnAs film with 4% Mn content. The photoexcited carriers were generated/probed at 3.467 μm, close to the fundamental gap of InMnAs, at 290 and 77 K and several relaxation regimes, after the initial increase in the differential transmission (DT) was observed. Optical transitions in semiconductors can be strongly influenced by the distribution of carriers in the conduction and valence bands. The initial sharp increase in the DT results from free carrier Drude absorption; whereas, the alteration of the dielectric function of the film through changes in the electron and hole distribution function can be responsible for the sign change of the DT. As shown in Fig. 1(b), by tuning the pump/probe at 3.1 μm, the DT demonstrated a different pattern and at 77 K the photoexcited carriers, in the time scale of ∼2 ps, fully relaxed to its initial value at negative time delay.

In the presence of point defects and midgap states, nonlinear absorption dynamics can influence the relaxation process, where the observed fast decay could be due to trapping of carriers in the midgap states and the slow component could be reflecting the slow recombination of the trapped carriers. In addition, in a degenerate pump-probe scheme when the pump/probe excitations are from the same source, the optical excitation of the carriers, followed by fast relaxation in the bands, can result in a saturation of the band-to-band absorption.[15,16] In order to avoid possible nonlinear effects, we employed nondegenerate differential transmission and examples of the measurements are presented.

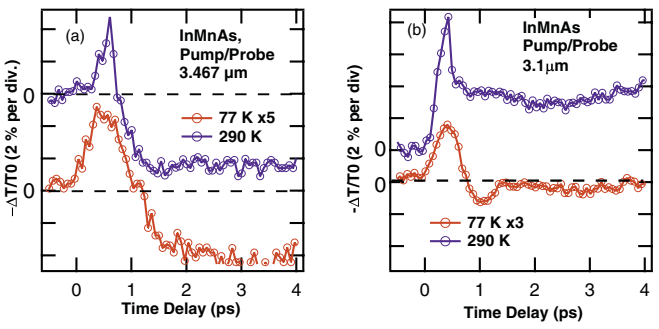

FIG. 1. (Color online) (a) DT- in MOVPE-grown ferromagnetic InMnAs at 290 and 77 K with pump/probe fixed at 3.467μm. (b) A different pattern in the relaxation was observed for the pump/probe at 3.1 μm.

III. NONDEGENERATE DIFFERENTIAL TRANSMISSION

In our nondegenerate differential transmission (NDDT) scheme the pump pulses were tuned above the fundamental gap. In this scheme, the photoexcited carriers were created by NIR pulses fixed at 800 nm above the InMnAs fundamental gap and probed by laser pulses ranging from 1.3–3.8 μm. The pump fluence was tunable from 1–5 mJ cm^{-2} corresponding to a photoexcited carrier density in the range of $\sim 5 \times 10^{18} - 1 \times 10^{19}$ cm^{-3}, respectively. The band structure calculations, presented in Sec. IV, show the optical transitions for a pump wavelength of 800 nm.

Figure 2 demonstrates the two-color differential transmission measurements in an InMnAs ferromagnetic film at 290 K for different pump fluences. The fast component of the temporal evolution can be attributed to the relaxation of the hot electrons and holes, and the slower component is attributed to the electron-hole recombination across the gap. In the regime of high electron densities, due to the screening effect and hot phonons, the hot electrons experience a significant reduction in their energy loss rate through the emissions of LO phonons; therefore, the relaxation time of the hot electrons increase at higher laser fluences.[17] In addition, some of the photoexcited electrons are energetically able to scatter between the X, L, and Γ valleys in the conduction band resulting in a longer and more complex relaxation dynamics.[18,19] The threshold for L-valley scattering in this sample is discussed in Sec. IV.

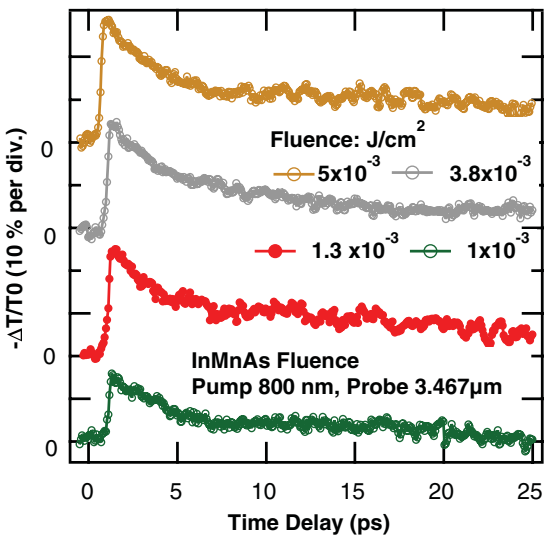

FIG. 2. (Color online) Two-color differential transmission measurements in InMnAs ferromagnetic film at 290 K and different pump fluences. The pump/probe pulses were 800 nm and 3.467 μm, respectively. The peak of the DT, $-\Delta T/T_0 = (T_0 - T)/T_0$, increases from 30% to ∼60%, suggesting larger photoinduced absorption at higher laser fluences.

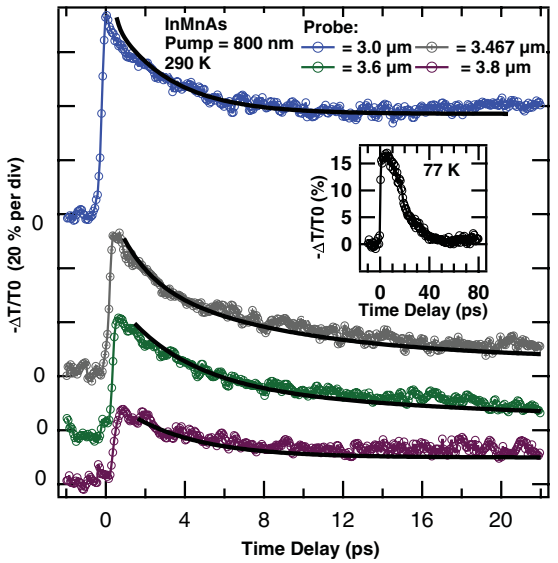

FIG. 3. (Color online) Two-color differential transmission measurements in InMnAs ferromagnetic film at 290 K for different probe wavelengths in MIR. The relaxation dynamic is dominated by photoinduced absorption. The exponential fits are shifted for clarity. The inset demonstrates an example of the measurements at 77 K for pump/probe at 800 nm/3.467 μm, respectively.

The reabsorption of the trapped carriers in the mid gap levels are responsible for the long relaxation time of the observed photoinduced absorption.[20,21] The photoexcited electrons in the conduction band can return to the valence band through the defect and midgap states. The trapped electrons act as an additional absorption center and could be reexcited to the conduction band after absorbing the probe beams. Except for the lowest laser fluence, the photoinduced carriers were not fully relaxed in a time scale longer than 10 ps.

As shown in Fig. 3, for the pump fixed at 800 nm, and a fluence of 3.8 mJ cm^{-2}, tuning the probe wavelengths in MIR resulted in several differences in the TRDT patterns, where both the amplitude and relaxation time demonstrate strong wavelength dependence. The $-\Delta T/T_0$ change, at 3.0 μm, exceeded 60%, suggesting larger photoinduced absorption compared to 3.8 μm in which the band filling could be more dominant. The gradual increase in the amplitude of the TRDT peak as a function of wavelength originated from band-gap renormalization which is important for probe energies around the band gap.

As demonstrated in the inset of Fig. 3, lowering the temperature to 77 K increased the relaxation time. If the reexcitation of the trapped electrons can influence and increase the relaxation of the photoinduced carriers, then the thermal fluctuations at higher temperatures make it harder to trap the photogenerated electrons, resulting in a faster relaxation compared to the observation at 77 K.

Our observations in the NDDT scheme in InMnAs were dominated by photoinduced absorption only for wavelengths longer than 2.6 μm. For several NIR probe pulses, ranging from 1.3 to 2.6 μm, we instead observed photoinduced bleaching. Figure 4 demonstrates examples of the photoinduced bleaching at different temperatures in InMnAs for the pump/probe tuned at 800 nm/2 μm, respectively. The

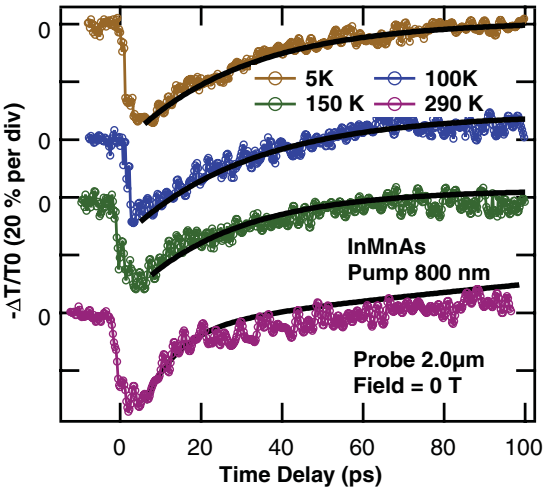

FIG. 4. (Color online) Two-color DT measurements of InMnAs ferromagnetic film at several temperatures. The pump and probe pulses were 800 nm and 2 μm, respectively. The photoinduced bleaching is dominating the temporal evolution of the DT.

temperature dependence of the observed photoinduced bleaching is not strong and the relaxation in this case lasts longer than the photoinduced absorption process. Due to the *Pauli exclusion* principle, photoexcited electrons in the conduction band and holes in the valence band can reduce the interband optical transitions via band and state filling. This leads to a decrease in the absorption and a corresponding increase in the transmission, which is referred to as bleaching. In a study by Kim *et al.*,[21] the sign of the differential reflectivity demonstrated a wavelength dependence in GaMnAs structures where point defect induced absorption is a possible mechanism.

While the TRDT is sensitive to the initial states and the band structure, we have tested a scheme where the photoexcited carriers were generated by pumping the GaAs substrate followed by a similar measurement on the ferromagnetic layer side. As shown in Fig. 5 the nature of the relaxations are different suggesting the strong dependence of the dynamics to the characteristics of the system under study. Unlike the case for Fig. 5(a), in Fig. 5(b), the carriers are excited from the GaAs and experienced different relaxation process compared with carriers originating from the ferromagnetic layer.

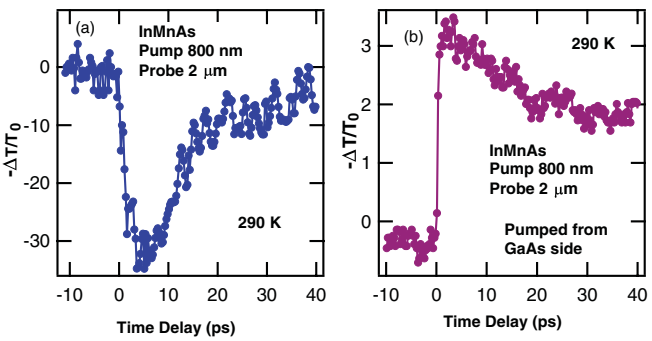

FIG. 5. (Color online) Two-color DT measurements of the InMnAs ferromagnetic film in two different configurations and relaxation dynamics. (a) When the film is pumped from the ferromagnetic side. (b) When the film is pumped from the GaAs side.

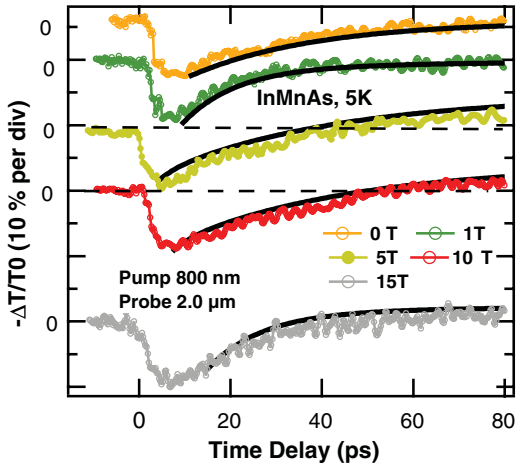

FIG. 6. (Color online) Two-color DT signals from InMnAs at different applied fields at 5 K. The exponential fits are shifted for clarity.

The observed wavelength dependence motivated us to probe the possibility of tuning the nature of the relaxation dynamics in the presence of external magnetic fields. In this case, the optical components inside the magnet were only compatible for probe pulses tuned below 2 μm with the pump pulses at 800 nm. Examples of our measurements at 5 K are presented in Fig. 6, where the photoinduced bleaching mainly dominated the temporal evolution of the DT. For external fields of 5 and 10 T, the photoinduced bleaching changes sign at a time delay of ~40 ps. Tuning the wavelengths around the band edge (3.0–3.8 μm) did not result in any change in the DT; however, applying an external field of 5 T, where the band structure is more complicated, caused the switch in the sign.

IV. CALCULATION OF ELECTRONIC STRUCTURE

To understand the effects of the ferromagnetic order on the electronic structure and subsequently the carrier relaxation dynamics, the electronic structure for bulk InMnAs has been calculated. Our preliminary calculations have focused on the band structure. By calculating the electronic band structure, we can determine where photoexcited carriers are generated by the pump pulse and which regions of the electronic structure are sampled by the probe pulse. Later, we will focus on the carrier dynamics. The calculations are based on an eight-band $\mathbf{k}\cdot\mathbf{p}$ model, which includes the conduction and valence band mixing. The model is similar to the Pidgeon-Brown model, which we have previously used to calculate electron states and to interpret cyclotron resonance experiments. In this situation, however, there is *no external magnetic* field but we allow for k_x and k_y dependencies. We use the standard eight $\mathbf{k} = 0$ Bloch basis states (two spin states each for the conduction band, heavy-hole, light hole, and spin-split valence band states) with no external magnetic field. We, however, include the effects of the spontaneous magnetization of the Mn ions and the *sp-d* coupling of this magnetization to the electrons and holes. This will spin split the bands even with no external magnetic field, provided the Mn ions are ferromagnetically ordered. The magnetization of the Mn ions is calculated using mean-field theory,[22–25] and the z component of the average Mn spin $< S_z >$ is determined by solving

$$< S_z >= SB_s\left\{\frac{gS}{kT}\left[\mu_B B - \frac{3kT_c < S_z >}{gS(S+1)}\right]\right\}, \qquad (1)$$

where B is the external magnetic field, g is the free electron g factor, B_s is the Brillouin function, $S = 5/2$ is the spin of the magnetic Mn ion, and $T_c = 330$ K is the Curie temperature. Figure 7 shows the calculated band structure for $In_{0.96}Mn_{0.04}As$ at 290 K for $T_c = 300$ K. We see that the ferromagnetic order of the Mn ions causes spin splitting of the bands. The red arrows in Fig. 7, show the optical transitions that are possible for an 800 nm pump pulse. We see that transitions are possible from the heavy-hole, light-hole, and spin-orbit split valence bands. Furthermore, the transitions from the heavy and light holes create photoexcited electrons in the conduction band that are above the energy threshold for scattering into the satellite L valleys. These electrons rapidly scatter into the satellite valleys (which have a large effective mass and hence a greater density of states) and take a long time to return to the Γ valley and then relax to the bottom of the Γ valley, similar to the 620 nm photoexcitation in GaAs.[26–28]

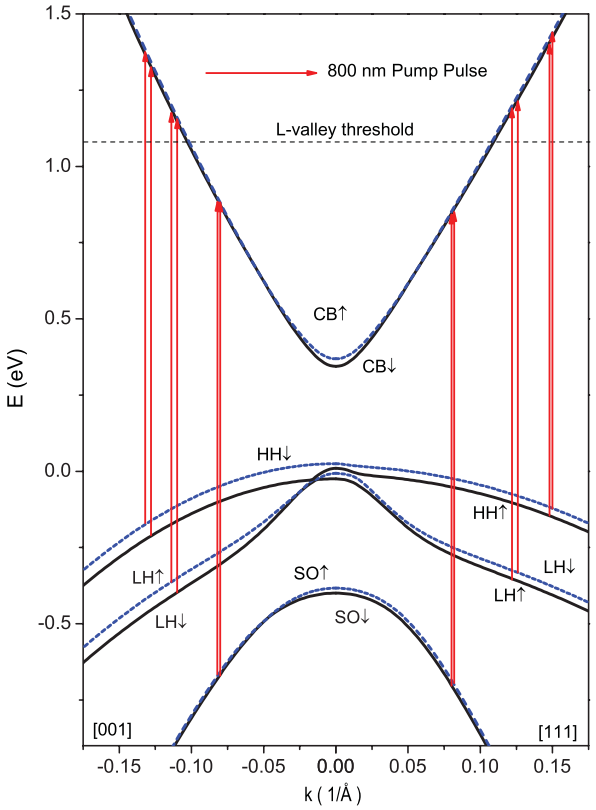

FIG. 7. (Color online) Electronic structure of $In_{0.96}Mn_{0.04}As$ at $T = 290$ K for $B = 0$, along the [001] and [111] directions. The energy bands are spin-split due to the ferromagnetism. The allowed optical transitions for a pump wavelength of 800 nm (1.55 eV) are shown by the (red) arrows. The dotted line at 1.08 eV shows the threshold for Γ valley electrons to scatter to the satellite L valley.

V. CONTRIBUTIONS TO THE DIFFERENTIAL TRANSMISSION SPECTRA.

The time-resolved DT measures *changes* to the absorption of the probe pulse that result from the pump pulse. For thin samples, $\Delta T/T \approx -\Delta\alpha\, L$, where L is the thickness of the sample and $\Delta\alpha$ is the change in the absorption coefficient. While a detailed understanding of the absorption changes requires using the semiconductor Bloch equations,[29] one can gain insight into what types of processes influence the DT signal by looking at a simplified, approximate expression for the absorption coefficient:

$$\alpha(\omega,t) = \frac{1}{\omega}\int d\omega' \int dt' N(\omega',t-t') \sum_{\text{transitions}} \int dk \underbrace{|H_k|^2}_{\substack{\text{optical}\\ \text{matrix}\\ \text{element}}} \times \delta[\underbrace{\varepsilon_c(k)-\varepsilon_v(k)}_{\substack{\text{electron and hole}\\ \text{energies}}} - \omega'][1-\underbrace{f_c^e(k,t')-f_v^h(k,t')}_{\substack{\text{electron and hole}\\ \text{distribution functions}}}]. \quad (2)$$

Here, $\alpha(\omega,t)$ is the absorption of the probe pulse centered at frequency ω as a function of delay time t with respect to the pump pulse, $N(\omega',t)$ is the transient photon energy density of the probe pulse, $H_{kk'}$ is the optical matrix element between conduction and valence band states, and $f_c^e(k,t')$ and $f_v^h(k,t')$ are the electron and hole distribution functions in the conduction and valence bands, respectively.

There are four main contributions to the differential transmission signal $-\Delta T/T_0 = (T_0 - T)/T_0$.[30] These can be understood by looking at changes in the absorption coefficient of the probe, Eq. (2) above, and seeing what changes as a result of the pump pulse. The four main contributions are the following. (1) Phase-space filling: this comes from the probe pulse creating additional electrons and holes that block the absorption of additional carriers from the probe pulse by the *Pauli exclusion principal*. One can not create an additional electron-hole pair with the probe pulse if the pump pulse has already created one since the Pauli principle excludes two electrons from being in the same state. As the photoexcited carriers relax, the absorption of the probe pulse increases with time. Phase space filling gives a negative contribution to $-\Delta T/T_0$ (provided there is no carrier inversion before the pump pulse). (2) Band-gap renormalization: this results from the pump pulse photoexciting electron-hole pairs, which through the many-body interactions, cause the electron and hole energies [in the delta function in Eq. (2)] to change. This causes the band gap to shrink. Band-gap renormalization gives a positive contribution for probe laser energies *below* the pump-induced photoexcited carriers and a negative contribution at energies *above* the pump-induced photoexcited carriers. This effect tends to be strong just below the band edge. With no pump pulse, probing below the band edge will not lead to absorption of the probe pulse. However, with a pump pulse, the band gap narrows and the probe pulse will now be absorbed. (3) Local field effects: photoexcited electon-hole pairs interact through the Coulomb interaction. This leads to the formation of excitons and changes to the electron and hole wave functions. (Even states excited above the band gap are *unbound excitons*). These changes to the wave functions will change the optical matrix elements in Eq. (2) and lead to a *Coulomb enhancement* of the absorption of the probe pulse. Now with a pump pulse on, additional electron-hole pairs are created that screen the Coulomb interaction and change the optical matrix elements. This gives a negative contribution at energies below the photoexcited carriers and a positive contribution at energies above the photoexcited carries. (4) Free carrier absorption: this is due to the *intraband* absorption of the photoexcited carriers (which must be assisted by phonons or impurities). This will give a positive contribution to $-\Delta T/T_0$ due to the photoinduced absorption.

Figure 8 shows the calculated bands of In $_{0.96}$Mn$_{0.04}$As at 290 K for $T_c = 300$ K. This time we show the transitions from the probe pulse. This allows us to see which regions are being monitored by the probe pulse. Transitions are shown for probe wavelengths of 3.5 μm (black arrows) and 2 μm (red arrows). We see that the 3.5 μm probe primarily probes the states at or near the band edge while the 2.0 μm probe is deep into the bands. This can explain the sign change in the differential transmission signal shown in Fig. 5.

From Fig. 8, we see the reason for the change of the sign between 3.5 and 2 μm. The 2 μm probes deep into the bands were the phase space filling contribution to $-\Delta T/T_0$ is dominant. However, the 3.5 μm transitions probe close to and slightly below the band edge. In this case, the band gap renormalization term will dominate and

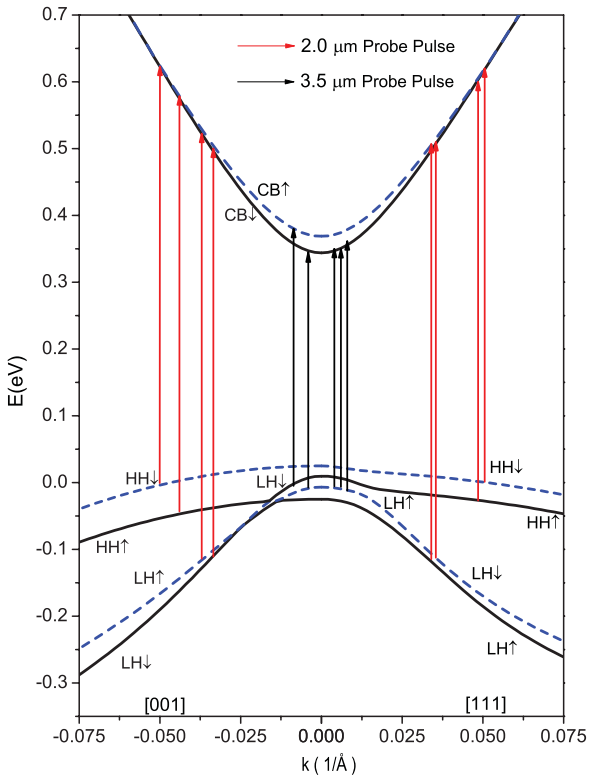

FIG. 8. (Color online) Electronic structure of In$_{0.96}$Mn$_{0.04}$As at $T = 290$ K for $B = 0$. The energy bands are spin-split due to the ferromagnetism. The allowed optical transitions are shown for a *probe* wavelength of 3.5 μm (black arrows) and 2.0 μm (red arrows).

give a positive signal to $-\Delta T/T_0$. In addition, free carrier absorption can also contribute to the observed positive signal at 3.5 μm.

In summary, we probed and tuned the carrier dynamics in the MOVPE grown InMnAs. In contrast to the reported studies in MBE grown InMnAs, focused on narrower pump/probe schemes,[12] the TRDT measurements in this work demonstrated that the carrier relaxation time can be tuned and last longer than a few picoseconds, when the excited carriers are close or above the L-valley threshold. In addition, we observed the change in the nature of the dynamical processes, switched between the photoinduced absorption and bleaching in a ferromagnetic semiconductor. We have calculated the electronic structure for InMnAs using an eight-band $\mathbf{k}\cdot\mathbf{p}$ model that includes the nonparabolicity and coupling of the electrons and holes to the Mn impurities, to model the observed dynamics. The calculated band structure with the bands splitting due to the Mn impurities shows that (1) the 800 nm pump pulse creates photoexcited carriers from all the hole bands and some of the photoexcited electrons can scatter to the satellite L valleys that slows down the relaxation of the electrons. (2) The sign change between probing with 3.5 and 2.0 μm can be explained by what regions of the bands are sampled by the probe pulses. At 2.0 μm, the probe is deep into the bands where the *phase-space-filling* term dominates. At 3.5 μm, the probe is right at and slightly below the band-edge where band-gap renormalization dominates.

ACKNOWLEDGMENTS

This work has been supported by the National Science Foundation through grants Career Award DMR-0846834, DMR-0800479, DMR-0706313, DMR-1105437, and by the National High Magnetic Field Laboratory through a UCGP. A portion of this work was performed at the National High Magnetic Field Laboratory, which is supported by National Science Foundation Cooperative Agreement No. DMR-0654118, the State of Florida, and the US Department of Energy. C.J. Stanton acknowledges DOE support (DE-FG02-02ER45984).

*Corresponding author: khoda@vt.edu

[1] T. Schallenberg and H. Munekata, Appl. Phys. Lett. **89**, 042507 (2006).
[2] A. J. Blattner and B. W. Wessels, Appl. Surf. Sci. **221**, 155 (2004).
[3] A. J. Blattner, P. L. Prabhumirashi, V. P. Dravid, and B. W. Wessels, J. Cryst. Growth **259**, 8 (2003).
[4] N. Rangaraju, P. Li, and B. W. Wessels, Phys. Rev. B **79**, 205209 (2009).
[5] N. D. Parashar, N. Rangaraju, V. K. Lazarov, S. Xie, and B. W. Wessels, Phys. Rev. B **81**, 115321 (2010).
[6] P. T. Chiu, S. J. May, and B. W. Wessels, Appl. Phys. Lett. **85**, 780 (2004).
[7] G. A. Khodaparast, M. Frazier, R. N. Kini, K. Nontapot, T. D. Mishima, M. B. Santos, and B. W. Wessels, Proc. SPIE **7608**, 76080O (2010).
[8] G. A. Khodaparast, M. Bhowmick, T. D. Mishima, M. B. Santos, C. Feaser, and B. W. Wessels, Spintronics III, Proc. SPIE **7760**, 77600X (2010).
[9] M. Bhowmick, T. R. Merritt, K. Nontapot, B. W. Wessels, O. Drachenko, and G. A. Khodaparast, Physics Procedia **3**, 1167 (2010).
[10] M. Frazier, K. Nontapot, R. N. Kini, G. A. Khodaparast, T. Wojtowicz, X. Liu, and J. K. Furdyna, Appl. Phys. Lett. **92**, 06191 (2008).
[11] K. Nontapot, R. N. Kini, A. Gifford, T. R. Merritt, G. A. Khodaparast, T. Wojtowicz, X. Liu, and J. K. Furdyna, Appl. Phys. Lett. **90**, 143109 (2007).
[12] J. Wang, C. Sun, Y. Hashimoto, J. Kono, G. A. Khodaparast, L. Cywinski, L. J. Sham, G. D. Sanders, C. J. Stanton, and H. Munekata, J. Phys. Condens. Matter **18**, R501 (2006).
[13] J. Wang, G. A. Khodaparast, J. Kono, A. Oiwa, and H. Munekata, J. Mod. Opt. **51**, 2771 (2004).
[14] R. N. Kini, K. Nontapot, G. A. Khodaparast, R. E. Welser, and L. J. Guido, J. Appl. Phys. **103**, 064318 (2008)
[15] P. P. Paskov and L. I. Pavlov, Appl. Phys. B **54**, 113 (1992).
[16] H. Kurz, Semicond. Sci. Technol. **7**, 124 (1992).
[17] T. Tsai, C. Chang, and S. Gwo, Appl. Phys. Lett. **90**, 252111 (2007).
[18] M. Ulman, D. W. Bailey, L. H. Acioli, F. G. Vallee, C. J. Stanton, E. P. Ippen, and J. G. Fujimoto, Phys. Rev. B **47**, 10267 (1993).
[19] A. V. Kuznetsov, Kim, Chang Sub, and C. J. Stanton, J. Appl. Phys. **80**, 5899 (1996).
[20] U. Siegner, R. Fluck, G. Zhang, and U. Keller, Appl. Phys. Lett. **69**, 2566 (1996).
[21] S. Kim, E. Oh, J. U. Lee, D. S. Kim, S. Lee, and J. K. Furdyna, Appl. Phys. Lett. **88**, 262101 (2006).
[22] G. A. Khodaparast, J. Kono, Y. H. Matsuda, S. Ikeda, N. Miura, Y. J. Wang, T. Slupinski, A. Oiwa, H. Munekata, Y. Sun, F. V. Kyrychenko, G. D. Sanders, and C. J. Stanton, Physica E **21**, 978 (2004).
[23] G. D. Sanders, Y. Sun, F. V. Kyrychenko, C. J. Stanton, G. A. Khodaparast, M. A. Zudov, J. Kono, Y. H. Matsuda, N. Miura, and H. Munekata, Phys. Rev. B **68**, 165205 (2003).
[24] M. A. Zudov, J. Kono, Y. H. Matsuda, T. Ikaida, N. Miura, H. Munekata, G. D. Sanders, Y. Sun, and C. J. Stanton, Phys. Rev. B **66**, 161307(R) (2002).
[25] N. W. Ashcroft and N. D. Mermin, *Solid State Physics* (Saunders College, Philadelphia, 1976), pp. 715–718.
[26] C. J. Stanton, D. W. Bailey, and K. Hess, Phys. Rev. Lett. **65**, 231 (1990).
[27] D. W. Bailey, C. J. Stanton, and K. Hess, Phys. Rev. B **42**, 3423 (1990).
[28] C. J. Stanton and D. W. Bailey, Phys. Rev. B **45**, 8369 (1992).
[29] H. Haug and S. Koch, *Quantum Theory of the Optical and Electronic Properties of Semiconductors* (World Scientific, Singapore, 1990).
[30] K. El Sayed and C. J. Stanton, Phys. Rev. B **55**, 9671 (1997).